Exploring two Higgs doublet models through Higgs production

Chien-Yi Chen and S. Dawson

Phys. Rev. D **87**, 055016 — Published 18 March 2013

DOI: 10.1103/PhysRevD.87.055016

Exploring Two Higgs Doublet Models Through Higgs Production

Chien-Yi Chen and S. Dawson

Department of Physics, Brookhaven National Laboratory, Upton, New York, 11973

(Dated: February 22, 2013)

Abstract

We discuss the connections between the recently observed Higgs-like particle and rare B decays in the context of two Higgs doublet models (2HDMs). The measured decays of the Higgs boson to fermions and gauge bosons, along with the observation of the decay $B_s \to \mu^+\mu^-$, place stringent restrictions on the allowed parameter space of 2 Higgs doublet models. Future measurements of $h^0 \to \gamma\gamma$ can potentially exclude type I 2HDMs, while the parameters of other 2HDMs are already severely restricted. The recent observations of the $h^0 \to \tau^+\tau^-$ and $h^0 \to b\overline{b}$ decays further constrain the models.

I. INTRODUCTION

The discovery of a Higgs-like particle at the LHC with a mass $m_{h^0} \sim 125\ GeV$ is the beginning of the exploration of the source of electroweak symmetry breaking. The new particle has been observed in a number of different final states with rates roughly consistent with the Standard Model predictions, although the decay rate to $\gamma\gamma$ is slightly high. The crucial task now is to extract the properties (spin/parity and couplings to fermions and gauge bosons) of this particle as precisely as possible and determine whether they correspond to those predicted by the minimal Standard Model. It is also important to explore the possibility that there is a spectrum of Higgs-like states.

Many beyond the Standard Model (BSM) scenarios have a Higgs-like particle which has Standard Model -like couplings to fermions and gauge bosons in the low energy limit, and precision measurements of the Higgs particle couplings can serve to limit the parameters of BSM models. A well motivated extension of the Standard Model is obtained by adding a second $SU(2)_L$ Higgs doublet, leading to 5 physical Higgs particles: h^0, H^0, A^0, and $H^{\pm}$. We will consider the possibility that the particle observed at the LHC is the lightest neutral Higgs particle, h^0, of a 2 Higgs doublet model (2HDM.)[1]

The 2HDM models generically have tree level flavor changing neutral currents (FCNCs) from Higgs exchanges unless there is a global or discrete symmetry which forbids such interactions[4, 5] and therefore we consider only the class of models where there is a discrete Z_2 symmetry such that one of the fermions couples only to a single Higgs doublet. FCNCs are highly suppressed in this case and provide stringent limits on the parameters of the models. There are four possibilities for 2HDMs of this type which are typically called the Type I, Type II, Lepton Specific, and Flipped models[4]. We review the limits from FCNCs on these models, and determine the range of parameters consistent with the latest Higgs measurements at the LHC. Our goal is to study the extent to which LHC measurements in the Higgs sector can restrict the possibilities for 2HDMs. Previous works have examined the possibility of enhancing the branching ratio $h^0 \to \gamma\gamma$[1, 6, 7], and various other channels[8–12] in the 2HDMs and we discuss the implications of a measurement of $h^0 \to \gamma\gamma$ which differs from the Standard Model prediction and demonstrate the impact of the $h^0 \to b\overline{b}$ and

[1] The possibility that the observed particle is the heavier neutral Higgs particle, H^0, of a 2HDM has been examined elsewhere[1–3].

TABLE I: Neutral Higgs Couplings in the 2HDMs

	I	II	Lepton Specific	Flipped
g_{hVV}	$\sin(\beta-\alpha)$	$\sin(\beta-\alpha)$	$\sin(\beta-\alpha)$	$\sin(\beta-\alpha)$
$g_{ht\bar{t}}$	$\frac{\cos\alpha}{\sin\beta}$	$\frac{\cos\alpha}{\sin\beta}$	$\frac{\cos\alpha}{\sin\beta}$	$\frac{\cos\alpha}{\sin\beta}$
$g_{hb\bar{b}}$	$\frac{\cos\alpha}{\sin\beta}$	$-\frac{\sin\alpha}{\cos\beta}$	$\frac{\cos\alpha}{\sin\beta}$	$-\frac{\sin\alpha}{\cos\beta}$
$g_{h\tau^+\tau^-}$	$\frac{\cos\alpha}{\sin\beta}$	$-\frac{\sin\alpha}{\cos\beta}$	$-\frac{\sin\alpha}{\cos\beta}$	$\frac{\cos\alpha}{\sin\beta}$

TABLE II: Charged Higgs Couplings in the 2HDMs

	I	II	Lepton Specific	Flipped
λ_{tt}	$\cot\beta$	$\cot\beta$	$\cot\beta$	$\cot\beta$
λ_{bb}	$\cot\beta$	$-\tan\beta$	$\cot\beta$	$-\tan\beta$
$\lambda_{\tau\tau}$	$\cot\beta$	$-\tan\beta$	$-\tan\beta$	$\cot\beta$

$h^0 \to \tau^+\tau^-$ measurements. Finally, we show how the recent measurement of $B_s \to \mu^+\mu^-$ [13] serves to further restrict 2HDMs.

II. REVIEW OF 2HDMS

The Higgs sector of the 2HDMs is parameterized in terms of $\tan\beta \equiv \frac{v_2}{v_1}$, where v_1 and v_2 are the vacuum expectation values of the two Higgs doublets and satisfy $M_W^2 = g^2(v_1^2+v_2^2)/2$, and the angle α which diagonalizes the neutral Higgs mass matrix. The couplings of the lightest Higgs boson, h^0, to the Standard Model particles are parameterized as:

$$\mathcal{L} = -\Sigma_i g_{iih}\frac{m_i}{v}\overline{f}_i f_i h^0 - \Sigma_{i=W,Z} g_{hVV}\frac{2M_V^2}{v}V_\mu V^\mu h^0\,, \tag{1}$$

where $g_{iih} = g_{hVV} = 1$ in the Standard Model and $v = 246GeV$. The h^0 coupling to gauge bosons is the same for all four models considered here, while the couplings to fermions differentiates between the models. The Higgs Yukawa couplings normalized to their Standard Model values are summarized in Table I. The Standard Model couplings are obtained for $\sin(\beta-\alpha) = 1$, $\sin\alpha = -\cos\beta$, and $\cos\alpha = \sin\beta$. The charged Higgs-fermion couplings can

be written as,

$$\mathcal{L} = \frac{g}{\sqrt{2}M_W}\overline{t}\Big(\lambda_{tt}m_t P_L - \lambda_{bb}m_b P_R\Big)bH^+ - \frac{g}{\sqrt{2}M_W}\overline{\nu}\lambda_{ll}m_l P_R l H^+ + \text{h.c.} \tag{2}$$

where $P_{L,R} = \frac{1\mp\gamma_5}{2}$, m_l is the charged lepton mass and the coefficients λ_{ff} are given in Table II.

Perturbative unitarity of the Yukawa couplings is violated if

$$(y_i)^2 = \left(\frac{g_{iih}}{\sqrt{2}}\right)^2 \;>\; 4\pi\,. \tag{3}$$

For all models considered here this requires $\tan\beta > 0.28$. Model II and the Flipped model require $\tan\beta < 140$, while the Lepton-specific model has the limit $\tan\beta < 350$ from perturbative unitarity. Other bounds on perturbative unitarity have been derived by requiring that the quartic couplings in the scalar potential remain positive up to a high scale[14] and by considering the perturbative unitarity of gauge boson scattering[15]. These bound typically give much lower upper bounds on $\tan\beta$ than those derived from perturbative unitarity of the Yukawa couplings, but we will not consider them further since these limits can be evaded by postulating new physics at some high scale.

There are also strong bounds on the 2HDMs from precision electroweak measurements, which can be parameterized by the oblique parameters, S, T and U. In the limit, $M_{H^0}, M_A, M_{H^\pm} >> M_Z$ and subtracting the Standard Model contribution[16, 17],

$$\begin{aligned}
\alpha\Delta T \;=\; & \frac{1}{16\pi^2 v^2}\Bigg\{f(M_A^2, M_{H^\pm}^2) - \sin^2(\beta-\alpha)\Big(f(M_{H^0}^2, M_A^2) - f(M_{H^0}^2, M_{H^\pm}^2)\Big) \\
& - \cos^2(\beta-\alpha)\Big((f(M_{h^0}^2, M_A^2) - f(M_{h^0}^2, M_{H^\pm}^2)\Big)\Bigg\} + \mathcal{O}\left(\frac{M_Z^2}{M_{H^0}^2}, \frac{M_Z^2}{M_A^2}, \frac{M_Z^2}{M_{H^\pm}^2}\right), \\
\Delta S \;=\; & \frac{1}{12\pi}\Bigg\{\cos^2(\beta-\alpha)\left[\log\left(\frac{M_{H^0}^2 M_A}{M_{H^\pm}^2 M_{h^0}}\right) + g(M_{h^0}^2, M_A^2)\right] \\
& + \sin^2(\beta-\alpha)\left[g(M_{H^0}^2, M_A^2) - \log\left(\frac{M_{H^\pm}^2}{M_{H^0} M_A}\right)\right]\Bigg\} + \mathcal{O}\left(\frac{M_Z^2}{M_{H^0}^2}, \frac{M_Z^2}{M_A^2}, \frac{M_Z^2}{M_{H^\pm}^2}\right),
\end{aligned} \tag{4}$$

where

$$\begin{aligned}
f(x,y) \;=\; & \frac{x^2+y^2}{2} - \frac{x^2 y^2}{x^2-y^2}\log\frac{x^2}{y^2} \\
g(x,y) \;=\; & -\frac{5}{6} + \frac{2xy}{(x-y)^2} + \frac{(x+y)(x^2-4xy+y^2)}{2(x-y)^3}\log\left(\frac{x}{y}\right).
\end{aligned} \tag{5}$$

For $M_A = M_{H^0} = M_{H^\pm}$ and $M_A >> M_Z$,

$$\begin{aligned} \alpha\Delta T &\sim \mathcal{O}\left(\frac{M_Z^2}{M_A^2}\right) \\ \Delta S &\sim \frac{1}{12\pi}\cos^2(\beta-\alpha)\left[\log\left(\frac{M_A^2}{M_{h^0}^2}\right) - \frac{5}{6}\right], \end{aligned} \tag{6}$$

For $M_A = M_{H^0} = M_{H^\pm} \sim 1\ TeV$, ΔT provides no useful limit on $\sin(\beta-\alpha)$, while ΔS requires $\cos(\beta-\alpha) \sim 1$. The most significant restrictions come from B decays, as discussed in the next section.

The branching ratios to fermions in the 2HDMs are simply scaled from the couplings of Table I and the total h^0 decay width. We use the Standard Model branching ratios from the LHC Higgs cross section working group for $M_{h^0} = 125\ GeV$[18]:

$$\begin{aligned} \Gamma_{h^0}^{SM} &= 4.07\ MeV \\ BR(h^0 \to b\overline{b})^{SM} &= .577 \\ BR(h^0 \to \tau^+\tau^-)^{SM} &= .063 \\ BR(h^0 \to c\overline{c})^{SM} &= .029 \\ BR(h^0 \to W^+W^-)^{SM} &= .215 \\ BR(h^0 \to ZZ)^{SM} &= .026 \\ BR(h^0 \to \gamma\gamma)^{SM} &= 2.28 \times 10^{-3} \\ BR(h^0 \to gg)^{SM} &= .086\,. \end{aligned} \tag{7}$$

The total widths in the 2HDMs are given by,[2]

$$\begin{aligned} \frac{\Gamma_{h^0}^{2HDM}}{\Gamma_{h^0}^{SM}} &\sim .577 g_{hbb}^2 + .029 g_{hcc}^2 + .063 g_{h\tau\tau}^2 + .241\sin^2(\beta-\alpha) \\ &\quad + \frac{\Gamma(h^0\to\gamma\gamma)^{2HDM}}{\Gamma(h^0\to\gamma\gamma)^{SM}} + \frac{\Gamma(h^0\to gg)^{2HDM}}{\Gamma(h^0\to gg)^{SM}} + ... \end{aligned} \tag{8}$$

where we neglect other contributions which are smaller than the $h^0 \to \gamma\gamma$ branching ratio and assume that there is no new physics beyond the 2HDM.

The decay width to $\gamma\gamma$ is found using the exact form factors of Refs. [19, 20]. For

[2] We assume $g_{hWW} = g_{hZZ}$.

$M_{h^0} = 125\ GeV$, the dominant contributions are

$$\frac{[\Gamma(h^0 \to \gamma\gamma)]^{2HDM}}{[\Gamma(h^0 \to \gamma\gamma)]^{SM}} \sim \left\{ .28 g_{htt} - .004 g_{hbb} - .0036 g_{h\tau\tau} - 1.27 g_{hWW} \right\}^2 + \left\{ .0057 g_{hbb} + .0033 g_{h\tau\tau} \right\}^2 . \quad (9)$$

The tri-linear $h^0 H^+ H^-$ coupling is not enhanced by a mass factor, and we neglect its negligible contribution[21].

Similarly, the decay to gluons proceeds predominantly through top and bottom quark loops,

$$\frac{\Gamma(gg \to h^0)^{2HDM}}{\Gamma(gg \to h^0)^{SM}} = \left\{ 1.06 g_{htt} - .06 g_{hbb} \right\}^2 + \left\{ .086 g_{hbb} \right\}^2 . \quad (10)$$

For large $\tan\beta$, the b quark loop can contribute significantly to the $gg \to h^0$ production channel in Model II and the Flipped model. In our numerical studies, we include both the b and t contributions exactly in all cases .

Using the results given above, the production from gluon fusion and the following decay to $\gamma\gamma$ or to $f\overline{f}$ pairs can be described by,

$$\begin{aligned} R_{\gamma\gamma}^{ggF} &= \frac{[\sigma(gg \to h^0) BR(h^0 \to \gamma\gamma)]^{2HDM}}{[\sigma(gg \to h^0) BR(h^0 \to \gamma\gamma)]^{SM}} \\ R_{f\overline{f}}^{ggF} &= \frac{[\sigma(gg \to h^0) BR(h^0 \to f\overline{f})]^{2HDM}}{[\sigma(gg \to h^0) BR(h^0 \to f\overline{f})]^{SM}} . \end{aligned} \quad (11)$$

The Higgs signal from gluon fusion with the subsequent decay to $\gamma\gamma$ is shown in Fig. 1 for $\sqrt{S} = 8\ TeV$[3]. It is interesting to note that in Model I, it is not possible to obtain $R_{\gamma\gamma}^{ggF}$ larger than ~ 1.2, so a future measurement which confirms the current deviation of $R_{\gamma\gamma}^{ggF}$ from 1 could serve to exclude Model I[4]. For $R_{\gamma\gamma}^{ggF} > 1$, only a narrow region of $\alpha \sim -0.5$ can be obtained. The Lepton Specific model is similar to Model I at small $\tan\beta$, while at large $\tan\beta$ (for fixed non-zero α) the total width is enhanced by the large branching ratio to $\tau^+\tau^-$, which decreases $R_{\gamma\gamma}^{ggF}$. A value of $R_{\gamma\gamma}^{ggF} \sim 1.2$ is only consistent with the Lepton Specific model for $\alpha \sim 0$ and $\tan\beta > 8$. Model II and the Flipped model have similar predictions for $R_{\gamma\gamma}^{ggF}$ with a wide range of α and $\tan\beta$ values consistent with $R_{\gamma\gamma}^{ggF} \sim 1$.

The gluon fusion production with decay to $\tau^+\tau^-$ is shown in Fig. 2. In Model I and the Flipped model, the Standard Model rate can be obtained for small α, relatively independently of $\tan\beta$. Model II and the Lepton Specific model only approximate the Standard

[3] There is very little change going from $\sqrt{S} = 7\ TeV$ to $\sqrt{S} = 8\ TeV$.
[4] This has also been noted in Ref. [2].

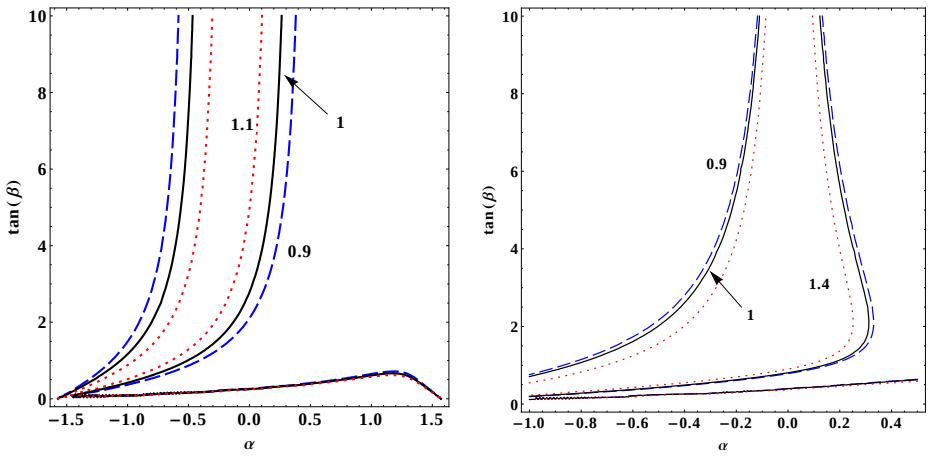

FIG. 1: The contours correspond to constant $R_{\gamma\gamma}^{ggF}$ as defined in the text for $\sqrt{S} = 8\,TeV$. For Type I (a): The blue (dashed), black (solid), and red (dotted) lines are $R_{\gamma\gamma}^{ggF} = .9, 1, 1.1$, respectively. For Type II (b): The blue, black, and red lines are $R_{\gamma\gamma}^{ggF} = .9, 1., 1.4$, respectively. For the Lepton Specific model (c): The blue, black, and red lines are $R_{\gamma\gamma}^{ggF} = .9, 1., 1.2$, respectively. For the Flipped model(d): The blue, black, and red lines are $R_{\gamma\gamma}^{ggF} = .9, 1., 1.4$, respectively.

Model rate for very specific values of α and $\tan\beta$ and hence a precise measurements of $R_{\tau\tau}^{ggF}$ can serve to restrict these models significantly.

Preliminary LHC measurements of $h^0 \to b\overline{b}$ and $h^0 \to \tau^+\tau^-$ in the vector boson fusion (VBF) and Vh^0 channels are particularly interesting and will serve to distinguish between the different 2HDMs. Both VBF and Vh^0 production follow the same simple scaling between

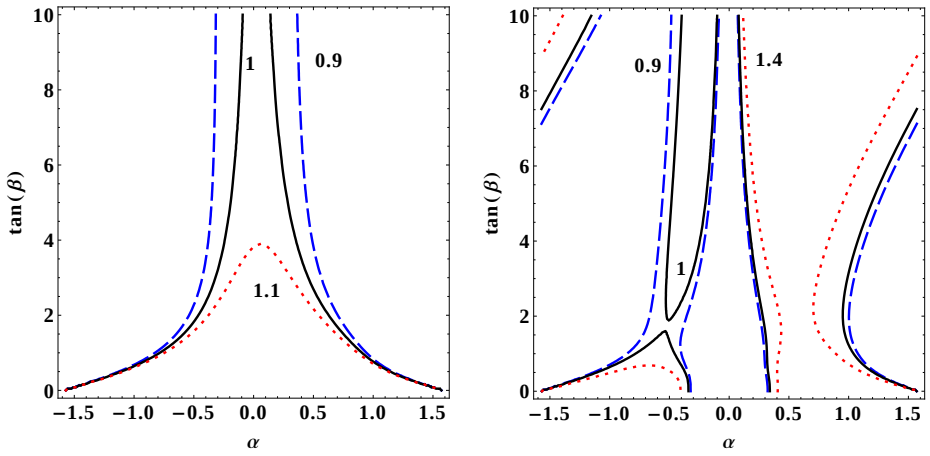

(a) (b)

(c) (d)

FIG. 2: The contours correspond to constant $R_{\tau\tau}^{ggF}$ as defined in the text for $\sqrt{S} = 8\,TeV$. For Type I (a): The blue (dashed), black (solid), and red (dotted) lines are $R_{\tau\tau}^{ggF} = .9, 1, 1.1$, respectively. For Type II (b): The blue, black, and red lines are $R_{\tau\tau}^{ggF} = .9, 1., 1.4$, respectively. For the Lepton-Specific model (c): The blue, black, and red lines are $R_{\tau\tau}^{ggF} = .9, 1., 1.2$, respectively. For the Flipped Model(d): The blue, black, and red lines are $R_{\tau\tau}^{ggF} = .9, 1., 1.4$, respectively.

the Standard Model rates and the 2HDM predictions,

$$R_{ff}^{VBF,Vh} \sim \sin^2(\beta - \alpha) g_{hff}^2 \,. \tag{12}$$

From Fig. 3, it is clear that the Standard Model rates, $R_{bb}^{VBF,Vh} \sim 1$ only occurs for very specific values of α and $\tan\beta$. In Model I and the Lepton Specific model, $R_{bb}^{VBF,Vh} \sim 1.1$ requires $\tan\beta < 1$, while Model II and the Flipped model require $\alpha \sim -0.5$ and $\tan\beta > 4-8$ for $R_{bb}^{VBF,Vh} \sim 1.4$. The rates to $\tau^+\tau^-$ normalized to the Standard Model predictions are

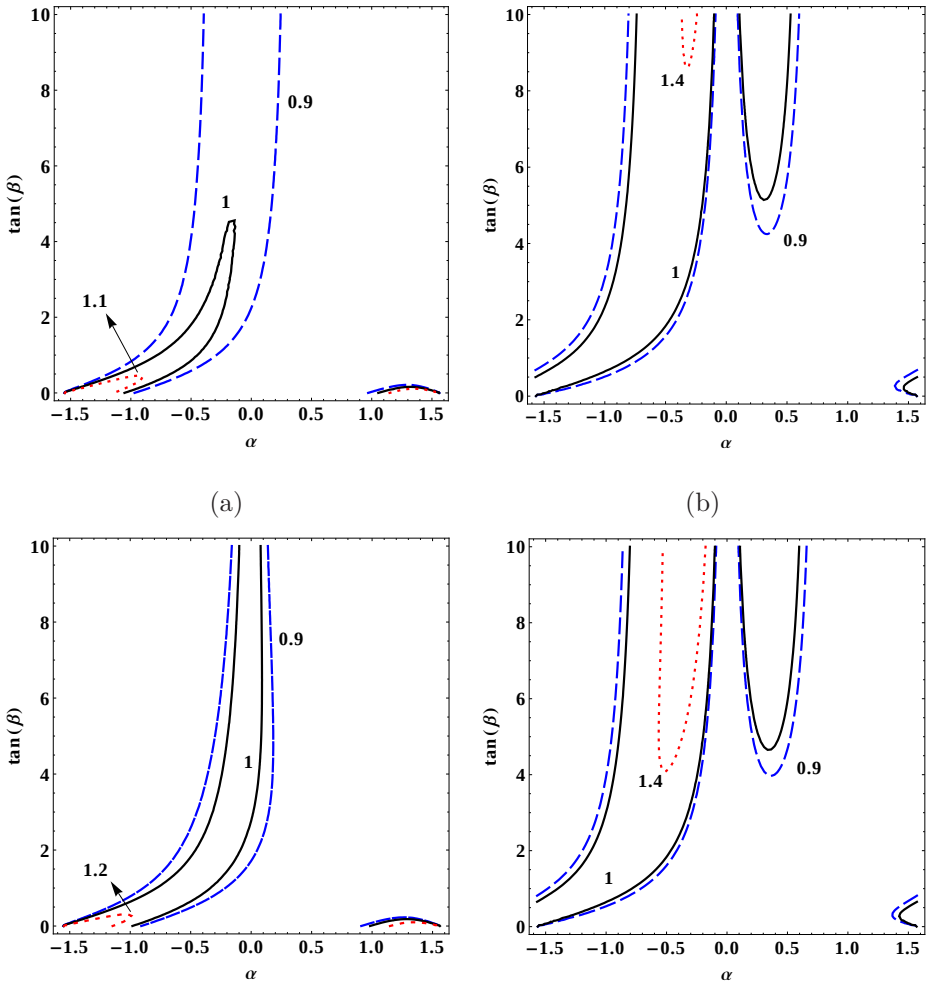

FIG. 3: The contours correspond to constant $R_{bb}^{VBF,Vh}$ as defined in the text. For Type I (a): The blue (dashed), black (solid), and red (dotted) lines are $R_{bb}^{VBF,Vh} = .9, 1, 1.1$, respectively. For Type II (b): The blue, black, and red lines are $R_{bb}^{VBF,Vh} = .9, 1., 1.4$, respectively. For the Lepton-Specific model (c): The blue, black, and red lines are $R_{bb}^{VBF,Vh} = .9, 1., 1.2$, respectively. For the Flipped Model(d): The blue, black, and red lines are $R_{bb}^{VBF,Vh} = .9, 1., 1.4$, respectively.

shown in Fig. 4. Note that in Models I and II, $R_{bb}^{VBF,Vh} = R_{\tau\tau}^{VBF,Vh}$. This is because the h^0 coupling to $b\overline{b}$ is the same as the h^0 coupling to $\tau^+\tau^-$ in these two models, as shown in Table I. As a result Fig. 3(a) is identical to Fig. 4(a) and similarly Fig. 3(b) and Fig. 4(b) are also identical to each other. One can also see that Fig. 3(a) and Fig. 3(c) are very similar since the coupling g_{hbb} for Model I and the Lepton-Specific model are the same. They are not identical because the total widths in these two models are different. This similarity also

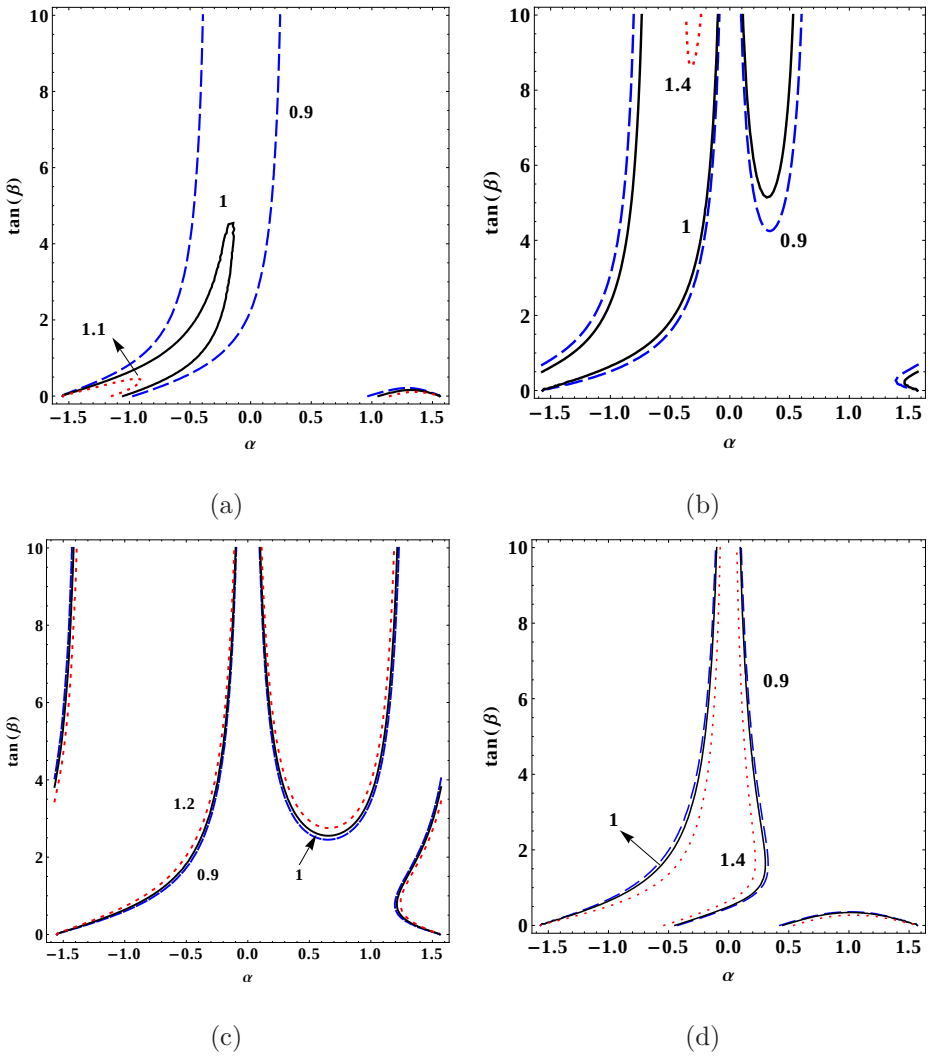

FIG. 4: The contours correspond to constant $R_{\tau\tau}^{VBF,Vh}$ as defined in the text. For Type I (a): The blue (dashed), black (solid), and red (dotted) lines are $R_{\tau\tau}^{VBF,Vh} = .9, 1, 1.1$, respectively. For Type II (b): The blue, black, and red lines are $R_{\tau\tau}^{VBF,Vh} = .9, 1., 1.4$, respectively. For the Lepton Specific model (c): The blue, black, and red lines are $R_{\tau\tau}^{VBF,Vh} = .9, 1., 1.2$, respectively. For the Flipped Model(d): The blue, black, and red lines are $R_{\tau\tau}^{VBF,Vh} = .9, 1., 1.4$, respectively.

appears in Fig. 3(b) and Fig. 3(d) because the h^0 coupling to $b\overline{b}$ is the same for Model II and the Flipped model.

III. REVIEW OF LIMITS FROM FLAVOR PHYSICS

Limits on 2HDMs have been examined by many authors and we briefly update the results of Ref. [22] using the SuperIso program[23–25] in order to examine the restrictions on

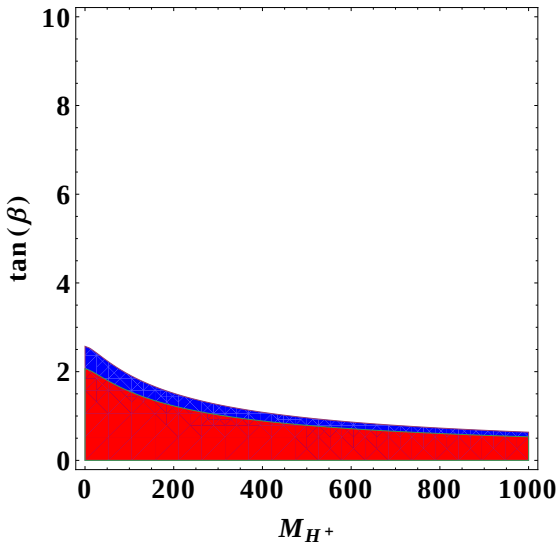

FIG. 5: Limits on 2HDMs from ΔM_{B_d}. Regions below the blue and red regions are excluded at 2 and 3σ, respectively.

$\tan\beta$ in the 2HDMs which are relevant for Higgs coupling studies. Small values of $\tan\beta$, $\tan\beta \lesssim 0.35$, for $M_{H^+} \lesssim 2\ TeV$ are excluded at 3σ in all 2HDMs considered here by the experimental measurement of ΔM_{B_d}[26],

$$\Delta M_{B_d}\ |_{exp}= 0.507 \pm 0.004\ ps^{-1}\,. \tag{13}$$

The limits from ΔM_{B_d} are identical in all 2HDMs studied in this work and the exclusion regions are shown in Fig. 5. For $M_{H^+} \sim 300\ GeV$, $\tan\beta < 1.03$ is excluded at 3σ. (For $M_{H^+} \sim 2\ TeV$, $\tan\beta < .35$ is excluded at 3σ.)

Stringent bounds also arise from the experimental measurement of $B \to X_s\gamma$[26, 27],

$$BR(B \to X_s\gamma)\ |_{exp}= (3.55 \pm 0.24 \pm 0.09) \times 10^{-4}\,, \tag{14}$$

and are shown in Fig. 6[22, 28]. For $M_{H^+} = 1\ TeV$, $\tan\beta < 0.69(0.16)$ is excluded at 3σ in Type I and the Lepton Specific model (Type II and the Flipped Model). For $M_{H^+} = 300\ GeV$ the restrictions are still fairly stringent: $\tan\beta < 1.36(0.88)$ is excluded at 3σ in Type I and the Lepton Specific model (Type II and the Flipped Model). For all values of $\tan\beta$, $M_{H^+} < 300\ GeV$ is excluded in the Type II and Flipped models. The numerical results agree with Refs. [22, 29–31] in the appropriate limits.

Finally, the recent observation of the decay $B_s \to \mu^+\mu^-$[13] has important implications

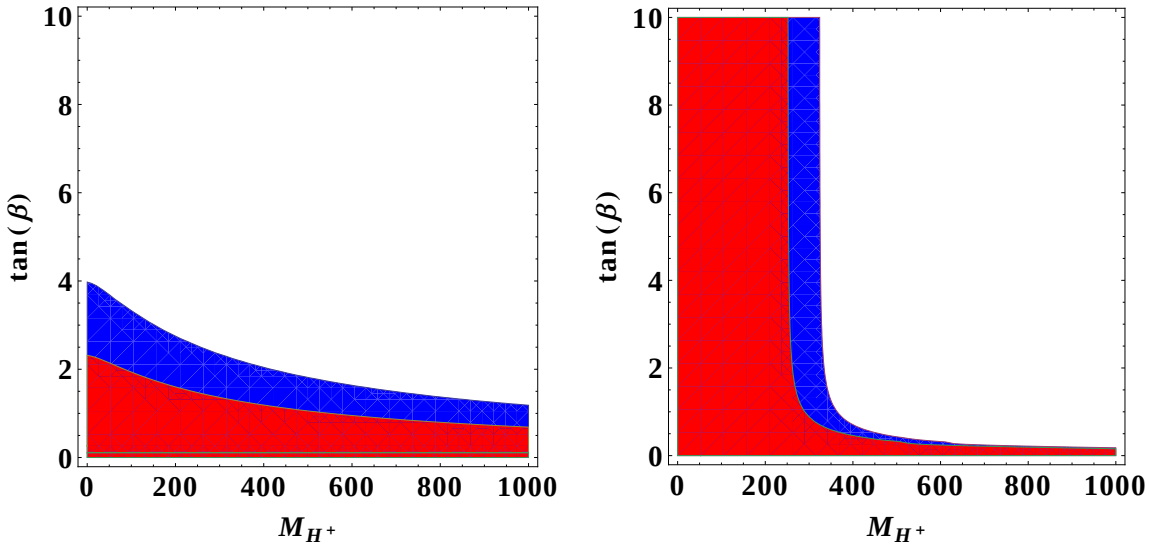

FIG. 6: Limits from the measurement of $B \to X_s\gamma$ in Type I and the Lepton Specific model (a). The regions below the blue (upper) and red (lower) curves are excluded at 2 and 3σ. The limits in Type II and the Flipped Model are in (b) and the regions to the left of the blue and red curves are excluded at 2 and 3σ, respectively.

for the 2HDMs,

$$BR(B_s \to \mu^+\mu^-)\,|_{exp} = (3.2^{+1.5}_{-1.2}) \times 10^{-9}\,, \tag{15}$$

in good agreement with the Standard Model prediction[32],

$$BR(B_s \to \mu^+\mu^-)\,|_{SM} = (3.23 \pm 0.27) \times 10^{-9}\,. \tag{16}$$

New physics effects in $B_s \to \mu^+\mu^-$ come predominantly from the charged Higgs exchanges and these effects are proportional to $\lambda_{tt}\lambda_{\mu\mu}$ as given in Table II. The contributions to $B_s \to \mu^+\mu^-$ in the type II Higgs doublet model have been computed in the large $\tan\beta$ regime in Refs. [33–35], and adapted to the general Two Higgs doublet models considered here in the SuperIso program[24].[5]

The branching ratio for $B_s \to \mu^+\mu^-$ in the Type I model is shown in Fig.7(a) as a function of M_{H^+} for various values of $\tan\beta$. It is apparent that for $M_{H^+} > 500$ GeV, the branching

[5] It is possible that there are contributions which are not enhanced by large $\tan\beta$ in the Type II model which could be relevant in the Type I, Lepton Specific or Flipped models. Such contributions are not included in the SuperIso program.

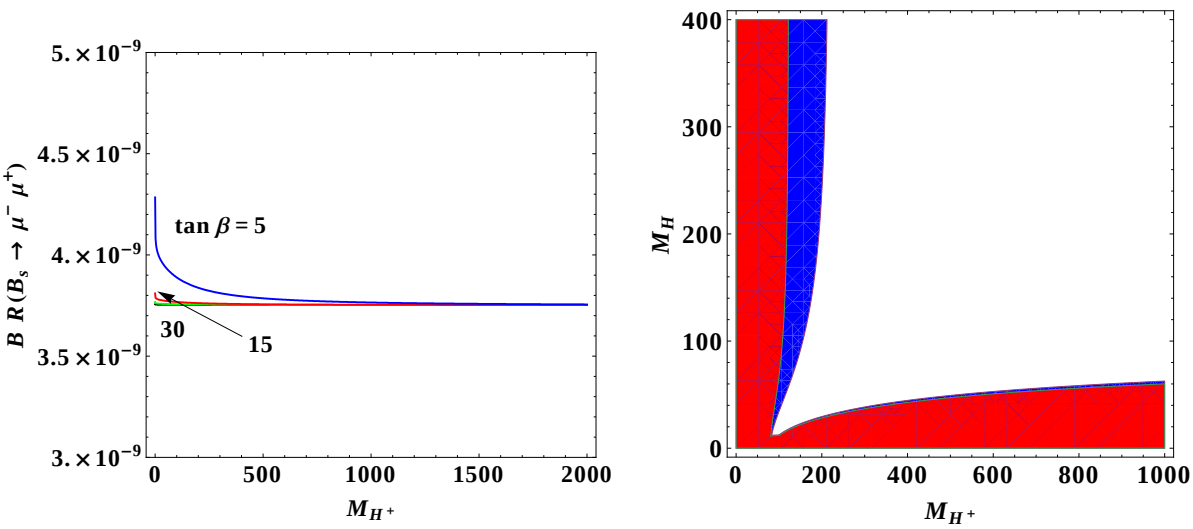

(a) (b)

FIG. 7: Branching ratios for $B_s \to \mu^+\mu^-$ in Model I (a) with $M_{H^0} = M_A = 300\ GeV$ for $\tan\beta$ =5 (blue), 15(red), and 30 (green). The excluded region from $B_s \to \mu^+\mu^-$ in Model I is shown in (b) with $M_{H^0} = M_A$. The red (blue+red) region of (b) is excluded at $3(2)\sigma$ for $\alpha = -0.88$ and $\tan\beta = 1$. These values of α and $\tan\beta$ correspond to the best fit to the Higgs data which is derived in Section IV. This plot, however, is rather insensitive to the precise value of $\tan\beta$.

ratio is almost a constant, independent of $\tan\beta$. In Fig.7(b), the excluded region is shown for the parameters which best fit the Higgs data (derived in the next section). However, for M_{H^+} and $M_H > 500$ GeV, the excluded region is not sensitive to the value of $\tan\beta$. Even for smaller values of M_{H^+} and M_H, the sensitivity to $\tan\beta$ is small.

In the Type II model, the branching ratio $B_s \to \mu^+\mu^-$ has a significant dependence on $\tan\beta$ for small M_{H^+}, and goes to a constant for very large M_{H^+}. In this model high values of $\tan\beta$ are excluded at 3σ for small M_{H^+}, while there is a 2σ excluded region at large $\tan\beta$, as shown in Fig. 8. The dependence of the excluded region on the choice of neutral Higgs masses, M_{H^0} and M_A, is shown in Fig. 9 for $\alpha = -0.02$ and $\tan\beta = 60$, (which corresponds to the best fit to the Higgs data derived in Section IV).

For the Lepton Specific case, the dominant contribution to $B_s \to \mu^+\mu^-$ is proportional to $\lambda_{tt}\lambda_{\mu\mu}$ and so the branching ratio is insensitive to $\tan\beta$. In Fig. 10, we show the $BR(B_s \to \mu^+\mu^-)$ as a function of M_{H^+} and the regions which are excluded at 2 and 3σ from this decay. We see that the excluded region does not depend on $\tan\beta$. For heavy charged Higgs masses, the branching ratio approaches a constant. The dependence on the choice of

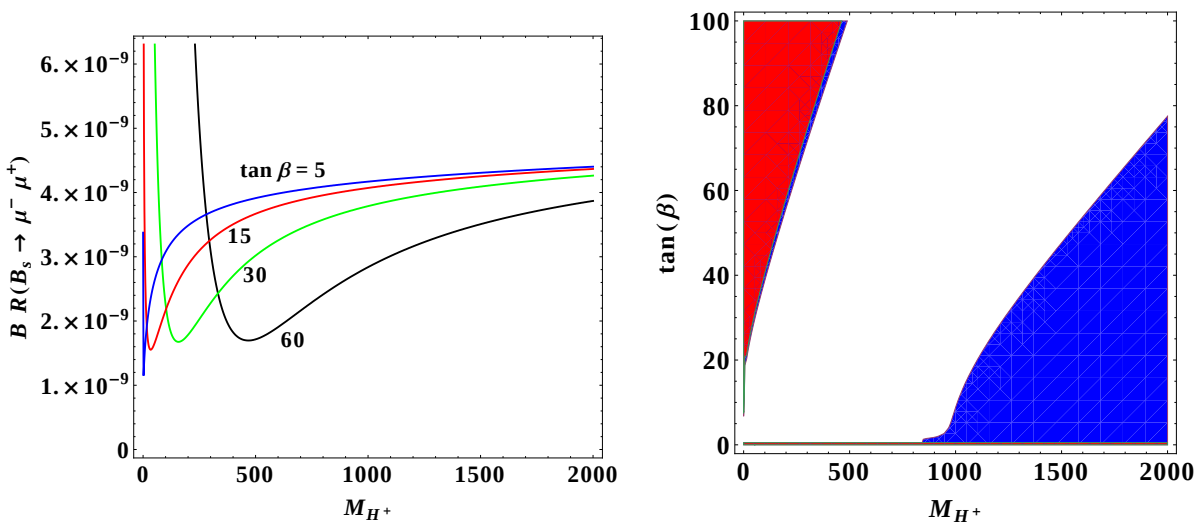

(a) (b)

FIG. 8: Branching ratios for $B_s \to \mu^+\mu^-$ in Model II (a) with $M_{H^0} = M_A = 300\ GeV$ for $\tan\beta$ =5 (blue), 15(red), 30 (green), and 60 (black). (At high M_{H^+}, $\tan\beta$ increases going from the top to bottom curves.) The excluded region from $B_s \to \mu^+\mu^-$ in Model II is shown in (b) with $M_{H^0} = M_A = 145\ GeV$. The red (blue+red) region of (b) is excluded at $3(2)\sigma$.

neutral Higgs masses is shown in Fig. 11. From Fig. 10(a), it is clear that the branching ratio for $B_s \to \mu^+\mu^-$ increases for $M_{H^+} \gtrsim 150$ GeV as M_{H^0} and M_A decrease. This leads to the exclusion of the region between $M_{H^0} = M_A \lesssim 100$ GeV and $M_{H^+} \gtrsim 150$ GeV at 2 σ in Fig. 11.

The branching ratio for $B_s \to \mu^+\mu^-$ for the Flipped model is shown in Fig. 12 for several values of $\tan\beta$ and for $M_{H^0} = M_A = 300\ GeV$. For $M_{H^+} > 300\ GeV$, the branching ratio is insensitive to the input parameters.

IV. RESULTS FROM HIGGS MEASUREMENTS

We do a simple χ^2 fit to the data shown in Tables III and IV assuming $M_{h^0} = 125\ GeV$. We follow the standard definition of $\chi^2 = \Sigma_i \frac{(R_i^{\rm 2HDM} - R_i^{\rm meas})^2}{(\sigma_i^{meas})^2}$, where R^{2HDM} represents predictions for the signal strength from the 2HDMs and $R^{\rm meas}$ stands for the most recent results of the measured signal strength shown in Tables III and IV by the ATLAS and CMS collabora-

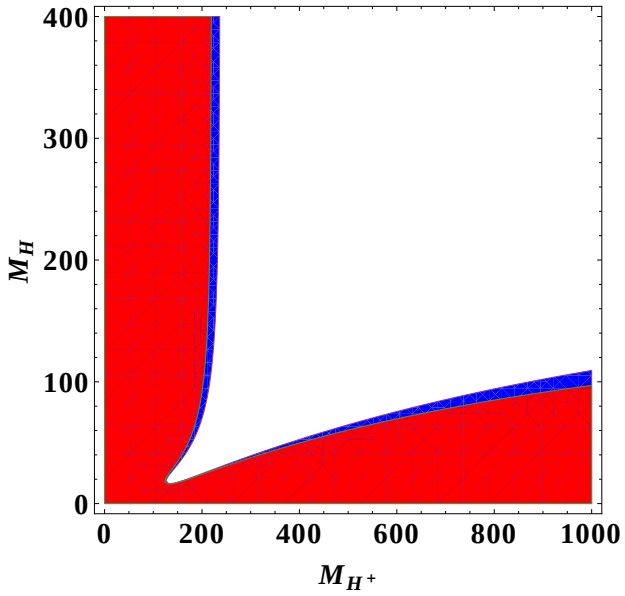

(a)

FIG. 9: Excluded region from $B_s \to \mu^+\mu^-$ in Model II with $M_{H^0} = M_A$ for $\alpha = -0.02$ and $\tan\beta = 60$. (These values of α and β correspond to the best fit to the Higgs data which is derived in Section IV.) The red (blue+red) region of is excluded at $3(2)\sigma$.

tions at the LHC. σ^{meas} denotes the uncertainty of R^{meas}.[6] The results (with no constraints from flavor physics) are shown in Fig. 13. In all cases, the χ^2 minima occurs for $\alpha \sim 1.3-1.4$ and $\tan\beta \sim 0.2-0.3$. The results of Sec. III, however, show that even for heavy M_{H^+} and heavy M_{H^0} and M_A, such small values of $\tan\beta$ are not allowed in the 2HDMs we consider here due to constraints from the B sector.

We perform a constrained fit to the data requiring $\tan\beta > 1$, which is consistent with B physics data of the previous section. In all models, the results of Fig. 13 show that there are large regions of parameter space allowed at both the 2 and 3σ confidence levels and the results have only a mild dependence on $\tan\beta$. In Model II and the Flipped model, $\alpha = 0$ is not allowed, primarily due to the $h^0 \to b\overline{b}$ measurement. In Model II, the Lepton Specific, and the Flipped model, only a small range of α is allowed and the χ^2 minimum occurs for

[6] The VBF tagged channels have a small contribution from gluon fusion. The ATLAS results (Table 1 of Ref. [36]) explicitly separate the true VBF contribution from the gluon fusion channel using Monte Carlo. The CMS VBF results of Ref. [45] (Table 1) contain a $30-50\%$ contamination from gluon fusion, estimated from Monte Carlo. We assume a 30% contamination of the CMS VBF result from gluon fusion, although the results of Fig. 13 are not sensitive to this assumption.

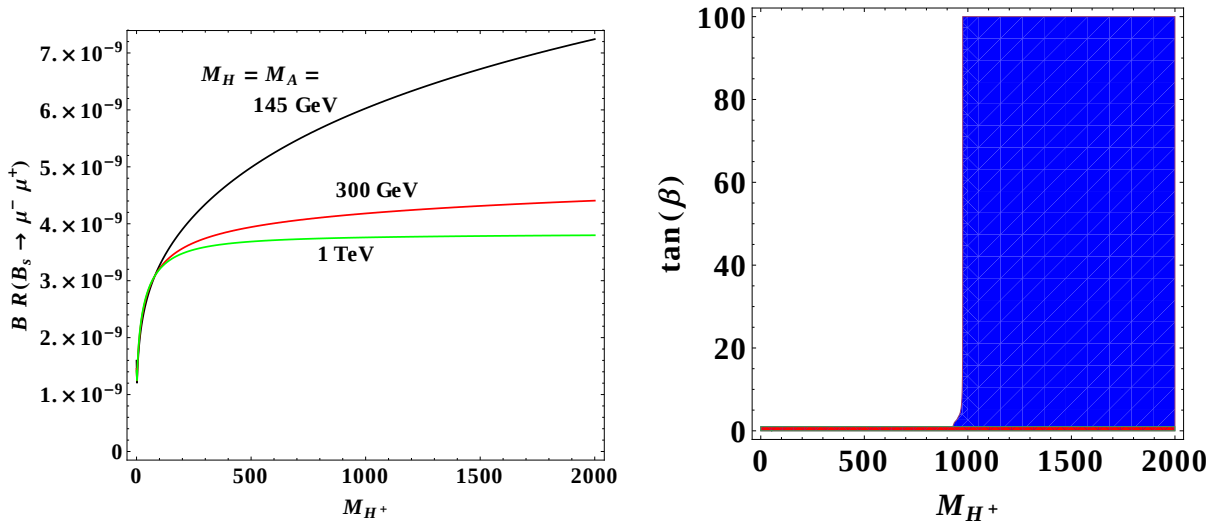

(a) (b)

FIG. 10: Branching ratios for $B_s \to \mu^+\mu^-$ in the Lepton Specific model (a). (The branching ratio is almost independent of $\tan\beta$.) The excluded region for $M_{H^0} = M_A = 145\ GeV$ is shown in (b). The red (blue+red) region of is excluded at $3(2)\sigma$.

large $\tan\beta$ (60, 54, and 77, respectively). In Model I, a fairly large range of α is consistent with the data and the χ^2 minimum is at $\tan\beta = 1$.

V. CONCLUSIONS

We have considered four variations of 2HDMs which have a Z_2 symmetry suppressing tree level FCNCs. Higgs production and decay in the 2HDMs can be significantly different than in the Standard Model and only small regions of $\alpha - \tan\beta$ can produce rates which are consistent with the experimental results from the LHC. Further, the parameters of these models are strongly constrained by measurements in the B sector. In particular, limits on ΔM_{B_d} require $\tan\beta \gtrsim 0.35$ for $M_{H+} \lesssim 2\ TeV$ in all 2HDMs considered here. For each model, we have also shown the regions in parameter space which are allowed by the measurement of $B_s \to \mu^+\mu^-$ for the parameters which correspond to the best fit to the Higgs data. Unitarity also restricts the allowed regions to have $\tan\beta \gtrsim 0.28$. Our major result is shown in Fig. 13 where we show the regions of $\alpha - \tan\beta$ which are consistent with the Higgs cross section and branching ratio results at the 2 and 3σ level. None of the models we studied can be excluded by current measurements.

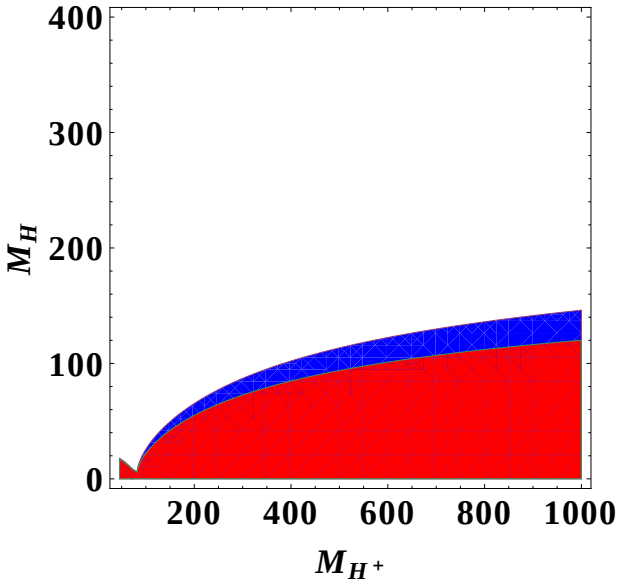

(a)

FIG. 11: Excluded region from $B_s \to \mu^+\mu^-$ in the Lepton Specific model with $M_{H^0} = M_A$ and $\alpha = -0.02$, the best fit to the Higgs data, derived in Section IV. (The excluded region is independent of $\tan\beta$.) The red (blue) region of is excluded at $3(2)\sigma$.

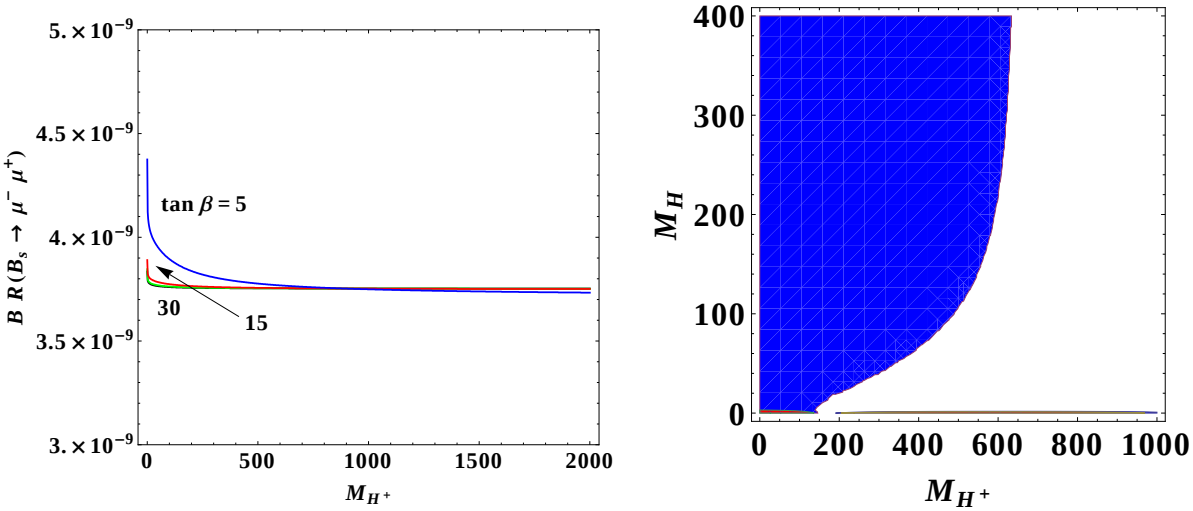

(a) (b)

FIG. 12: Branching ratios for $B_s \to \mu^+\mu^-$ in the Flipped model (a) with $M_{H^0} = M_A = 300\ GeV$ for $\tan\beta$ =5 (blue), 15(red), and 30 (green). Excluded region from $B_s \to \mu^+\mu^-$ in the Flipped model (b) (with $M_{H^0} = M_A$). The blue region of (b) is excluded at 2σ if we assume the uncertainty is five times smaller than the current one for $\alpha = -0.01$ and $\tan\beta = 76.56$, which corresponds to the best fit to the Higgs data derived in Section IV.

TABLE III: Measured Higgs Signal Strengths

Decay	Production	Measured Signal Strength R^{meas}
$\gamma\gamma$	ggF	$1.8 \pm 0.4 \pm 0.2 \pm 0.2$, [ATLAS] [36]
	VBF	$2.0 \pm 1.2 \pm 0.6 \pm 0.3$ [ATLAS][36]
	inclusive	1.8 ± 0.4 [ATLAS][37]
	ggF	1.4 ± 0.6 [CMS][38]
	VBF	$2.1^{+1.4}_{-1.1}$ [CMS][38]
	inclusive	1.56 ± 0.43 [CMS][38]
	ggF	$6.1^{+3.3}_{-3.2}$ [Tevatron][39]
WW	ggF	1.5 ± 0.6 [ATLAS] [37]
	ggF	0.74 ± 0.25 [CMS][40]
	VBF	$0.3^{+1.5}_{-1.6}$ [CMS][38]
	Wh	$-2.9^{+3.2}_{-2.9}$ [CMS][38]
	ggF	$0.8^{+0.9}_{-0.8}$ [Tevatron][39]
ZZ	inclusive	1.0 ± 0.4 [ATLAS][37]
	inclusive	$0.8^{+0.35}_{-0.28}$ [CMS][41]

TABLE IV: Measured Higgs Signal Strengths

Decay	Production	Measured Signal Strength R^{meas}
$b\bar{b}$	Vh	-0.4 ± 1.0 [ATLAS] [37]
	Vh	$1.3^{+0.7}_{-0.6}$ [CMS][42]
	Vh	$1.56^{+0.72}_{-0.73}$ [Tevatron][39]
$\tau^+\tau^-$	ggF	2.4 ± 1.5 [ATLAS][43]
	VBF	-0.4 ± 1.5 [ATLAS][43]
	inclusive	0.8 ± 0.7 [ATLAS][37]
	ggF	$0.9^{+0.8}_{-0.9}$ [CMS][44]
	VBF	0.7 ± 0.8 [CMS][44]
	Vh	$1.0^{+1.7}_{-2.0}$ [CMS][44]
	inclusive	0.72 ± 0.52 [CMS][44]
	ggF	$2.1^{+2.2}_{-1.9}$ [Tevatron][39]

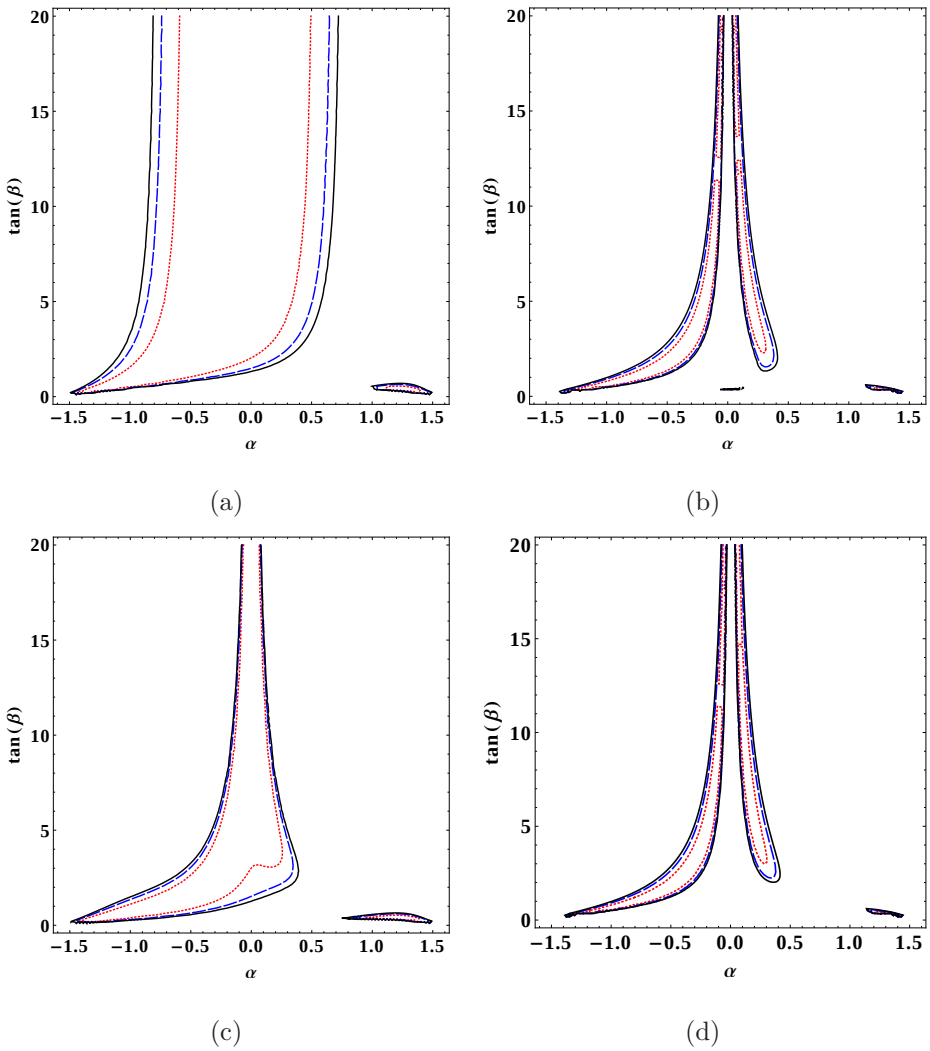

FIG. 13: Allowed regions in the $\alpha - \tan\beta$ plane in Type I (a), Type II (b), Lepton Specific (c), and Flipped (d) 2HDMs obtained by minimizing the χ^2 with no restrictions from flavor physics. The region between the black (solid), blue (dashed), and red (dotted) lines is allowed at 99%, 95%, and 68% confidence level.

Acknowledgements

We would like to thank Alejandro Celis, Nathaniel Craig, Kyle Cranmer, Jamison Galloway, Marc-Andre Pleier, Gabe Shaughnessy, and Scott Thomas for useful discussions. We also thank F. Mahmoudi for help with SuperIso. This work is supported by the United States Department of Energy under Grant DE-AC02-98CH10886.

---

[1] P. Ferreira, R. Santos, M. Sher, and J. P. Silva, Phys.Rev. **D85**, 035020 (2012), 1201.0019.

[2] A. Drozd, B. Grzadkowski, J. F. Gunion, and Y. Jiang (2012), 1211.3580.

[3] S. Chang, S. K. Kang, J.-P. Lee, K. Y. Lee, S. C. Park, et al. (2012), 1210.3439.

[4] G. Branco, P. Ferreira, L. Lavoura, M. Rebelo, M. Sher, et al., Phys.Rept. **516**, 1 (2012), 1106.0034.

[5] Y. Grossman, Nucl.Phys. **B426**, 355 (1994), hep-ph/9401311.

[6] P. Ferreira, R. Santos, M. Sher, and J. P. Silva, Phys.Rev. **D85**, 077703 (2012), 1112.3277.

[7] D. S. Alves, P. J. Fox, and N. J. Weiner (2012), 1207.5499.

[8] N. Craig and S. Thomas, JHEP **1211**, 083 (2012), 1207.4835.

[9] N. Craig, J. A. Evans, R. Gray, C. Kilic, M. Park, et al. (2012), 1210.0559.

[10] Y. Bai, V. Barger, L. L. Everett, and G. Shaughnessy (2012), 1210.4922.

[11] A. Azatov and J. Galloway, Int.J.Mod.Phys. **A28**, 1330004 (2013), 1212.1380.

[12] B. A. Dobrescu and J. D. Lykken (2012), 1210.3342.

[13] R. Aaij et al. (LHCb Collaboration) (2012), 1211.2674.

[14] S. Kanemura, T. Kasai, and Y. Okada, Phys.Lett. **B471**, 182 (1999), hep-ph/9903289.

[15] S. Kanemura, T. Kubota, and E. Takasugi, Phys.Lett. **B313**, 155 (1993), hep-ph/9303263.

[16] H. E. Haber and H. E. Logan, Phys.Rev. **D62**, 015011 (2000), hep-ph/9909335.

[17] H.-J. He, N. Polonsky, and S.-f. Su, Phys.Rev. **D64**, 053004 (2001), hep-ph/0102144.

[18] S. Dittmaier et al. (LHC Higgs Cross Section Working Group) (2011), 1101.0593.

[19] J. F. Gunion, H. E. Haber, G. L. Kane, and S. Dawson, Front.Phys. **80**, 1 (2000).

[20] A. Djouadi, Phys.Rept. **459**, 1 (2008), hep-ph/0503173.

[21] J. F. Gunion and H. E. Haber, Phys.Rev. **D67**, 075019 (2003), hep-ph/0207010.

[22] F. Mahmoudi and T. Hurth (2012), 1211.2796.

[23] F. Mahmoudi, Comput.Phys.Commun. **178**, 745 (2008), 0710.2067.

[24] F. Mahmoudi, Comput.Phys.Commun. **180**, 1579 (2009), 0808.3144.

[25] F. Mahmoudi, Comput.Phys.Commun. **180**, 1718 (2009).

[26] E. Barberio et al. (Heavy Flavor Averaging Group) (2008), 0808.1297.

[27] B. Aubert et al. (BABAR Collaboration), Phys.Rev. **D77**, 051103 (2008), 0711.4889.

[28] F. Mahmoudi and O. Stal, Phys.Rev. **D81**, 035016 (2010), 0907.1791.

[29] M. Baak, M. Goebel, J. Haller, A. Hoecker, D. Ludwig, et al., Eur.Phys.J. **C72**, 2003 (2012), 1107.0975.

[30] H. E. Logan and D. MacLennan, Phys.Rev. **D79**, 115022 (2009), 0903.2246.

[31] H. E. Logan and D. MacLennan, Phys.Rev. **D81**, 075016 (2010), 1002.4916.

[32] A. J. Buras, J. Girrbach, D. Guadagnoli, and G. Isidori, Eur.Phys.J. **C72**, 2172 (2012), 1208.0934.

[33] H. E. Logan and U. Nierste, Nucl.Phys. **B586**, 39 (2000), hep-ph/0004139.

[34] C. Bobeth, T. Ewerth, F. Kruger, and J. Urban, Phys.Rev. **D64**, 074014 (2001), hep-ph/0104284.

[35] J. R. Ellis, K. A. Olive, and V. C. Spanos, Phys.Lett. **B624**, 47 (2005), hep-ph/0504196.

[36] ATLAS Collaboration, ATLAS-CONF-2012-168.

[37] ATLAS Collaboration, ATLAS-CONF-2012-170.

[38] CMS Collaboration, CMS PAS HIG-12-020.

[39] See talk slides, 'H $\to$ bb from Tevatron', by Yuji Enari, at HCP2012.

[40] CMS Collaboration, CMS PAS HIG-12-042.

[41] CMS Collaboration, CMS PAS HIG-12-041.

[42] CMS Collaboration, CMS PAS HIG-12-044.

[43] ATLAS Collaboration, ATLAS-CONF-2012-160.

[44] CMS Collaboration], CMS PAS HIG-12-043.

[45] CMS Collaboration, CMS PAS HIG-12-045.